Prediction and Rationalization of Site Preference of Rare Earth Elements in Fluorapatite from Density Functional Theory

Smahane Dahbi[1], Angelika D. Rosa,[2] Alain Manceau*[1,2] and Stephan N. Steinmann*[1]

[1]CNRS, ENS de Lyon, LCH, UMR 5182, 69342, Lyon cedex 07, France
[2]European Synchrotron Radiation Facility (ESRF), 38000 Grenoble, France

Corresponding authors: alain.manceau@ens-lyon.fr; stephan.steinmann@ens-lyon.fr

ABSTRACT

Fluorapatite (FAp, nominally $Ca_{10}(PO_4)_6F_2$) has been identified as an important host-material for rare earth elements and yttrium (REY) in marine sediments. REY can be accommodated in either the larger 6+3 coordinated Ca1 site or the smaller 6+1 coordinated Ca2 site, yet little is known about the site preference of REY through the lanthanide series despite its importance for understanding REY enrichment processes in FAp. Theoretical investigations based on density functional theory (DFT) predict that all REY intrinsically prefer the smaller and more ionic Ca2 site. The Ca2 site preference is less pronounced when the excess of positive charge resulting from the REY^{3+} for Ca^{2+} substitution is compensated by a coupled Na^{+} for Ca^{2+} substitution, instead of the energetically more favorable Si^{4+} for P^{5+} coupled substitution. The site preference varies quadratically with the ionic radius of REY and linearly with the sum of their first and second ionization energies. The quadratic shape of the site preference is similar to the shape of Onuma diagrams, which suggests that the local effective elastic constant of the site controls the site preference, rather than the nominal size of the site. Despite being smaller, the Ca2 site has a lower effective elastic constant, and is, therefore, more flexible than the Ca1 site for accommodating larger and smaller trivalent REY cations. Concentration-dependent computations show that REY clustering is thermodynamically favorable, except for Yb and Lu.

KEYWORDS: Apatite, REY, Onuma diagram, DFT, Ionic radii, Charge compensation, Concentration

INTRODUCTION

Incorporation of rare earth elements and yttrium (REY) in apatite ($Ca_{10}(PO_4)_6(OH,Cl,F)_2$) has been extensively studied in the past decades, when it was recognized that this mineral is the dominant host for REY in common magmatic/metamorphic rocks.[1,2] This topic has attracted renewed attention recently[3–7] after the discovery in 2011 of deep-sea muds rich in REY in the Pacific Ocean,[8] and the further identification in 2014 of fluorapatite (FAp) as their main host phase.[9] REY enrichment can reach ore-grade in FAp, and therefore marine deposits are considered a potential resource for strategic REY used in industrial and technological applications, such as permanent magnets, electronic equipment and catalysis.[10] Knowing the crystal chemistry of REY in FAp would help us unravel the geochemical formation conditions of this georesource and may help develop efficient extraction processes.

The crystal structure of FAp has two non-equivalent calcium sites.[11] The Ca1 site is 9-fold coordinated with oxygen atoms (d(Ca1-O) = 2.554 Å), and exhibits C_{3v} symmetry. The smaller Ca2 site is 7-fold coordinated with six oxygen atoms (d(Ca2-O) = 2.462 Å) and one fluorine atom (d(Ca2-F) = 2.311 Å, average = 2.440 Å), and exhibits C_s symmetry. The Ca1 polyhedra are linked to each other through faces and to Ca2 polyhedra through corners. In contrast, the Ca2 polyhedra are linked to each other through corners, not faces. In this way, the Ca1 polyhedra form rigid chains and the Ca2 polyhedra flexible spirals along the c-axis. The two different Ca chains are interlinked by PO_4 tetrahedra (**Figure 1)**.[12] Electron and laser probe micro-analysis of magmatic/hydrothermal apatite showed that REY are

incorporated in the crystal structure and substituted for Ca.[7] Three questions arise from this result: (1) in which Ca site are REY preferentially incorporated in the structure, (2) does the partitioning of REY among the two sites vary through the lanthanide series as a function of the REY concentration, and (3) how is the REY^{3+} for Ca^{2+} substitution charge compensated?

The three questions are regularly addressed in the literature, generally indicating that the nature of the sample (e.g., synthetic vs natural) may cause diverging results, although the Ca2 site is more commonly reported as the incorporation site of REY. In 1973, Mackie et al.[13] synthesized Nd-doped FAp with a concentration of about 14,000 ppm (mg/kg), which they characterized by single-crystal X-ray diffraction. They found that Nd occupies the two Ca sites when Nd is supplied as NdF_3 and only the Ca2 site when it is supplied as Nd_2O_3. Incorporation of Nd in the Ca2 site with Nd_2O_3 as dopant source was confirmed by Fleet et al.[14] in 1994 at a Nd concentration of 82,000 ppm. Preference of Nd for the Ca2 site is also predicted by density functional theory (DFT). Bertolus and Defranceschi[15] calculated in 2000 the thermodynamic stability of all possible structural configurations of $Ca_8NdNa(PO_4)_6F_2$ and $Ca_9Nd(PO_4)_5(SiO_4)F_2$. Na^+ and Si^{4+} were incorporated in the models to balance the excess of positive electric charge resulting from the Nd^{3+} for Ca^{2+} substitution. Nd was predicted to occupy the Ca2 site regardless of the charge compensation mechanism, whereas Na preferred the Ca1 site. X-ray powder diffraction and infrared spectroscopy were used by Get'man et al.[16] in 2010 to study the incorporation of Sm and Gd in hydroxyapatite (HAp, $Ca_{10-x}REY_x(PO_4)_6(OH)_{2-x}O_x$). Sm and Gd were both found in the Ca2 site. Luminescence emission of Eu^{3+} indicates that Er occupies the Ca2 site both in HAp ($Ca_{10-x}Er_{2x/3}\square_{x/3}(PO_4)_6(OH)_2$)[17] and in oxyapatite ($Ca_{10-x}La_{x-0.2}Eu_{0.2}(SiO_4)_6O_{x/2}\square_{4-x/2}$).

The relative preference of REY for the Ca1 and Ca2 sites through the REY series was studied on both natural and synthetic samples. In 1991, Hughes et al.[18] determined the structure of REY-containing natural apatite using single-crystal X-ray diffraction. They found that the light (i.e., larger) REE (La → Sm) have a marked preference for the smaller Ca2 site. This observation contrasts with bond valence calculation, which suggested that only La, Ce, and Pr are substituted preferentially at the Ca2 site, while Pm and Sm should preferentially occupy the Ca1 site. Fleet et al.[19] revisited this question in 1995 on synthetic FAp doped at 79,000 - 110,000 ppm using also single-crystal X-ray diffraction. They found that the Ca2/Ca1 site occupancy ratio decreases monotonically with the effective ionic radius (IR)[20,21] of the REE. For example, the Ca2/Ca1 ratio of La (^{VI}IR = 1.03 Å) was 4.04 and that of Dy (^{VI}IR = 0.91 Å) was 1.54. This trend is inconsistent with an IR effect only, because the Ca1 site is larger than the Ca2 site.

In summary, previous studies have shown that REY favor the Ca2 site with, however, some differences depending on the synthesis method (e.g., NdF_3 vs. Nd_2O_3), and suggested a possible trend in the relative preference of the lanthanides for the two sites, which remains unexplained.

Regarding the charge balance of the REY^{3+} for Ca^{2+} substitution, three main possibilities may exist: Ca vacancies, coupled cation or coupled anion substitution.[18,22,23] The two last are most relevant in the context of marine deposits as sodium ions and silica are present in seawater:

$$2\,Ca^{2+} \rightleftarrows REY^{3+} + Na^{+} \quad (1)$$

$$Ca^{2+} + P^{5+} \rightleftarrows REY^{3+} + Si^{4+} \quad (2)$$

Recently, we have studied the incorporation of Ce^{3+} in FAp using high energy-resolution fluorescence detected extended X-ray absorption fine structure (HERFD-EXAFS) spectroscopy and DFT.[24] We showed that Ce occupies the Ca2 site and that Na favors the Ca1 site at a doping concentration of ~15,000 ppm. In absence of meaningful reference energies for “free” Ca^{2+}, P^{5+}, Si^{4+} and Na^+ cations to balance chemical equations, the most favorable charge-compensation models were obtained by comparing their energies relative to those of reference structures in which Ce and the co-dopant are well-separated and thus minimally interacting. Using this scheme, we found that the charge compensation with a SiO_4^{4-} for PO_4^{3-} substitution (eq 2) is energetically more stable than that with a Na for Ca1 substitution (eq. 1). Furthermore, the coupled Ce^{3+}-Na^+ and Ce^{3+}-Si^{4+} substitutions preferentially take place at short distance in the FAp structure (e.g., edge-sharing CeO_7-SiO_4 linkage, Figure 1b). Site preference and ionization energies were correlated linearly for divalent cations. On the basis of the

atomic charge of divalent substituents, we found that the Ca2 site is more ionic, and therefore is preferred by dopants with low ionization energies (e.g. Ba) over those with higher ionization energies (e.g., Mg).

Here, we extend our previous study on Ce to the whole REY series and explore the effect of REY concentration, focusing on the two main charge-compensation mechanisms, i.e., Na and Si co-doping. We reveal an intrinsic preference of all REY for the Ca2 site which is enhanced by the Si-based charge balance. However, at high concentration REY can be stabilized in the Ca1 site if the charge is balanced by Na.

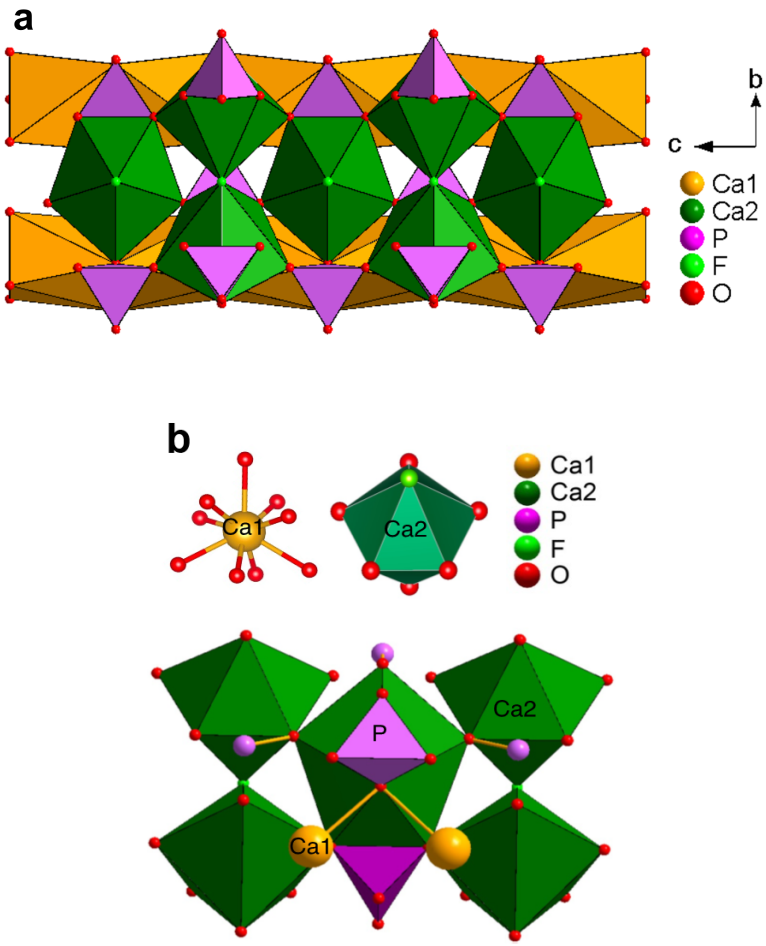

Figure 1: a) Polyhedral structure of FAp projected along the *c*-axis. b) Linkages of the Ca2 polyhedra.

COMPUTATIONAL METHODOLOGY

Geometry optimization of the pristine and doped FAp models was carried out using DFT,[25] in combination with Projector Augmented Wave (PAW) pseudopotentials[26,27] as implemented in the Vienna Ab-initio Simulation Package (VASP) software,[28,29] running on a Linux-based high-performance computing platform.[30] A plane-wave basis set with a kinetic energy cutoff of 500 eV was chosen, along with the generalized gradient approximation developed by Perdew, Burke, and Ernzerhof (PBE)[31] to describe the exchange-correlation potential, coupled with the density-dependent dispersion correction (dDsC).[32,33] The parameter controlling the convergence criterion for the electronic self-consistency cycle was set to 10^{-6} eV, and the maximum force convergence threshold was fixed to 0.05 eV/Å. An electronic Fermi-Dirac smearing with a width of 0.026 eV was used, but given the large band-gap of the materials studied, the smearing had no impact on the converged electronic structure. All relative and reaction energies discussed in this study refer to electronic energies. Calculation of free energies requires a

phonon computation, which is prohibitively expensive for the largest systems studied herein (1344 atoms), and an estimate of the configurational entropy at different REY concentrations.

FAp crystallizes in the hexagonal system with the $P6_3/m$ space group,[12] and the unit cell has 10 calcium (Ca), 6 phosphorus (P), 24 oxygen (O), and 2 fluorine (F) atoms. The REY concentration was varied by changing the size of the FAp cell. A single unit cell was used for the high concentration of about 100,000 ppm ($Ca_8REY_1Na_1(PO_4)_6F_2$ and $Ca_9REY_1(PO_4)_5(SiO_4)F_2$) (**Figure S1a)**, a 2 x 2 x 2 supercell for the intermediate concentration of about 12,500 ppm ($Ca_{78}REY_1Na_1(PO_4)_{48}F_{16}$ and $Ca_{79}REY_1(PO_4)_{47}(SiO_4)F_{16}$), as in our previous study[24] (**Figure S1b)**, and a 4 x 4 x 2 supercell for a concentration of about 3,125 ppm ($Ca_{318}REY_1Na_1(PO_4)_{192}F_{64}$ and $Ca_{319}REY_1(PO_4)_{191}(SiO_4)F_{64}$) (**Figure S1c)**. The unit cell is described by 3 x 3 x 3 K-points, and the supercells are probed at the gamma point. We verified that energies obtained with the unit cell and super-cell models were very similar (**Table S1)**. The dispersion-corrected PBE-dDsC functional was chosen over the Perdew-Wang[34] functional (PW91) used by Bertolus and Defranceschi[15] in their Nd-FAp study based on the comparison of the cell parameters for FAp obtained experimentally[12] and theoretically (**Table S2**). This is also in agreement with our previous study on Ce-doped FAp.[24] The deviation of the calculated *a* and *c* parameters relative to experiment is 0.5-0.6% with PW91 and <0.1% with PBE-dDsC. The accuracy on geometry is clearly better with PBE-dDsC. We note that after completion of the computations reported herein, a benchmark study has been published, recommending the use of dispersion corrections for simulating apatites[35] and that dispersion corrections have a long history in being used for apatites.[36] Additional spin-polarized DFT+U computations are included to the Supporting Information (**Figures S2**) which overall show similar results to the ones presented herein, but are plagued by difficult-to-converge wave functions and, thus, numerical noise. The effective Hubbard parameter (U-J) of 4 eV was applied to the REY f-orbitals as recommended by the open quantum materials database (OQMD).

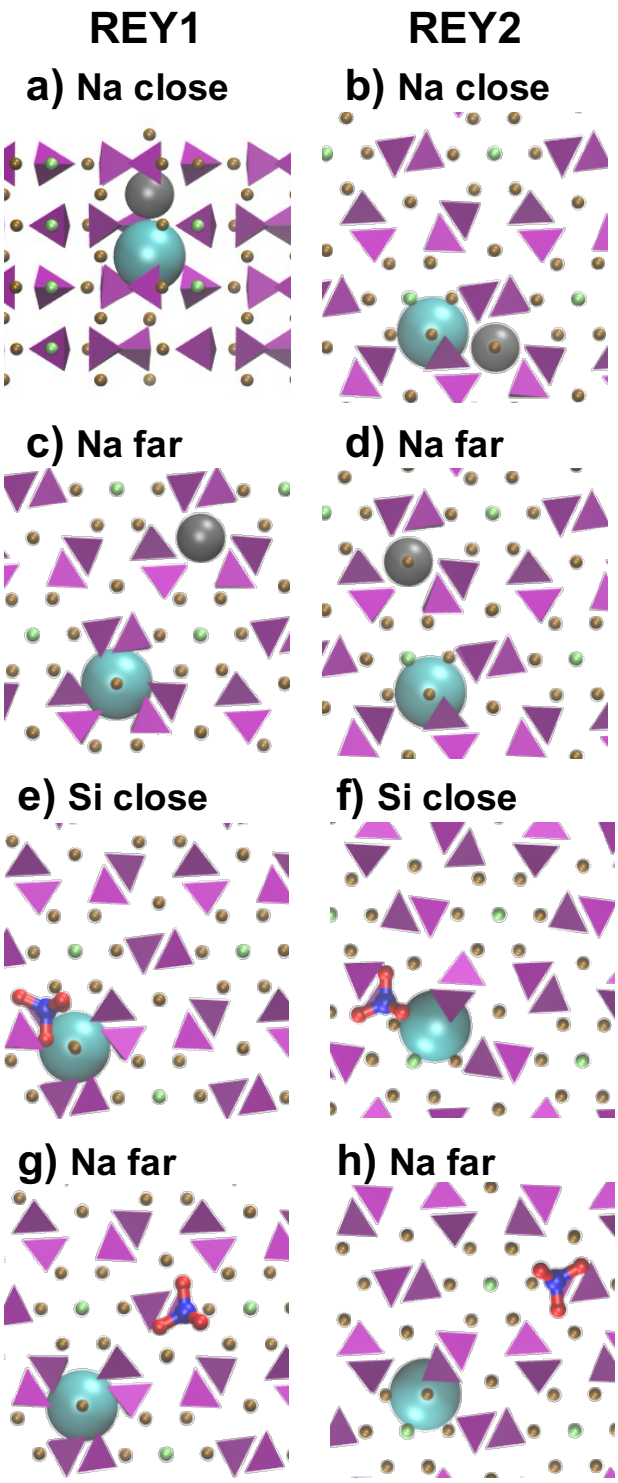

Figure 2: REY1 (left column) and REY2 (right column) models for "close" and "far" configurations. Specifically: Nd1,Na1 close (a) Nd2,Na1 close (b), Nd1,Na1 far (c), Nd2,Na1 far (d) Nd1,Si close (e), Nd2,Si close (f), Nd1,Si far (g), Nd2,Si far (h). Colorcode: purple: PO_4^{3-} groups, green: F, ochre: Ca, grey: Na, blue: Si, red: O.

RESULTS AND DISCUSSION

Charge Compensation. Previous DFT computations on Nd[15] and Ce[24] showed that the positive charge resulting from the REY^{3+} for Ca^{2+} substitution is balanced locally by a coupled Ce^{3+}-Na^{+} or Ce^{3+}-Si^{4+} substitution. This prior analysis was extended to all REY by calculating the difference in electronic energy between the "close" association of the REY and Na/Si dopants (distance <4 Å) and the well-

separated arrangement “far” (distance of ~9 Å and ~17 Å in the 2x2x2 and 4x4x2 supercells, respectively). The location of REY and the co-dopant are depicted in **Figure 2** for the 2x2x2 cell. Results are shown in **Figure 3** with the two models denoted “close” and “far” at a constant concentration of 12,500 ppm. The difference is always negative, meaning that the most stable arrangement is obtained when the REY and its co-substituent are in close contact, in agreement with the previous theoretical reports for Nd and Ce.[15,24] The gain in energy between the far and the close models is highest when REY occupy the Ca2 site (denoted REY2) with Si as co-dopant. When Na provides the charge-balance, it is the REY1 (REY in Ca1 site) substitution that gains the most energy. However, the additional stability procured for REY1 when Na is displaced from 9 Å (far) to the close position is generally not large enough to counterbalance the intrinsic preference of REY for the Ca2 site (seen in all well-separated arrangements, **Figure S3**). In addition, in absolute terms Na provides less stability than Si. This finding means that charge compensation is more efficient with Si than with Na, regardless of the REY site occupancy. A main reason for the difference between Si and Na is that the Si tetrahedron allows for charge compensation at shorter distance to the REY (d(REY1-Si)= 3.08 Å for a shared corner), d(REY2-Si)= 2.99 Å for a shared edge) than does Na (d(REY1-Na)= 3.41 Å, d(REY2-Na)= 3.96 Å)). Hence, Si maximizes the Coulombic interactions. The shorter REY1-Na distance compared to REY2-Na distance is also well in line with Na stabilizing the REY1 site. In summary, local charge compensation by Na partially counteracts the intrinsic Ca2 preference of REY, whereas Si further enhances it. In the following, all discussed coupled Na↔Ca and Si↔P substitutions refer to the “close” arrangement (distance < 4 Å), unless otherwise stated.

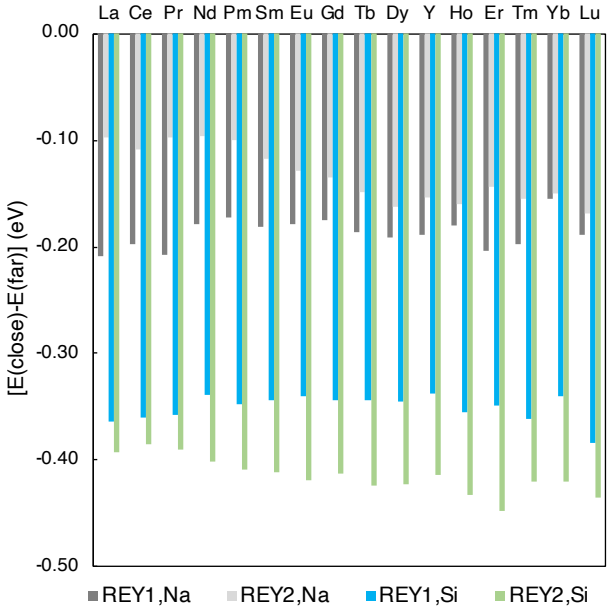

Figure 3: Energetic gain when moving the Na or Si co-dopant from ~9 Å (far) to close contact with REY at a REY concentration of 12,500 ppm. Dark and light grey bars indicate energetic gains for Na on either the REY1 or REY2 sites, while blue and green bars indicate those for Si on either the REY1 and REY2 sites, respectively.

Variation in Bond Distance and Cell Volume. The average REY1-O distances are greater than the average REY2-O distances, as observed for the Ca-O distances in FAp (d(Ca1-O) = 2.55 Å, d(Ca2-O) = 2.44 Å)[12] (**Figure 4**). In agreement with expectations, d(REY1-O) and d(REY2-O) decrease approximately linearly with IR along the REY series (R^2 = 0.84 and 0.89, respectively). Consistent with the IR values of the respective cations, substitution of REY for Ca enlarges the polyhedra volume for La and Ce whereas other REYs contract it. The REY1 and REY2 regression lines have a slope of 0.6 and 1.1, respectively, and 2.53 and 2.45 Å intersects. These values are the same for the Na and Si co-substitutions, within uncertainty of the regression. The two intersects agree well with the expectation that their values, corresponding to a zero difference in IR, match the size of the Ca sites. In other words,

the +II vs +III oxidation states of Ca and REY marginally influence the size of the site. Another significant result is that our computations reproduce the relative slopes of approximately 2:1 for the REY1 and REY2 sites obtained experimentally by Fleet and Pan based for four REY single-crystal X-ray diffraction measurements.[37] Clearly, the Ca1 site is "stiffer" than the Ca2 site (smaller slope of the linear regression), i.e., it does not adjust as easily to a change in the size of the dopant compared to the Ca2 site. This point will be of importance when discussing below the relative site preference and the connection to Onuma diagrams.

Fleet and Pan (1995)[37] observed that the unit-cell volume decreases when the average bond distance decreases in synthetic (La,Nd,Gd,Dy)-substituted FAp.[37] Consistent with this observation, we found that the difference of volume between the REY substituted and pure Ca FAp is strongly correlated (R^2 = 0.97) with the difference of IR between REY and Ca through the REY series (**Figure S4**). In contrast to the bond distance-IR relationship discussed previously, the intersect of the linear regression deviates significantly from zero (which would indicate identical volumes for REY and Ca FAp), especially for the Si co-substitution, suggesting non-negligible "dilation" compared to unsubstituted FAp for equal REY and Ca IR. This is likely related to the longer Si-O (~1.64 Å) vs P-O (~1.55 Å) bond. These findings attest to the physical soundness of the DFT analysis.

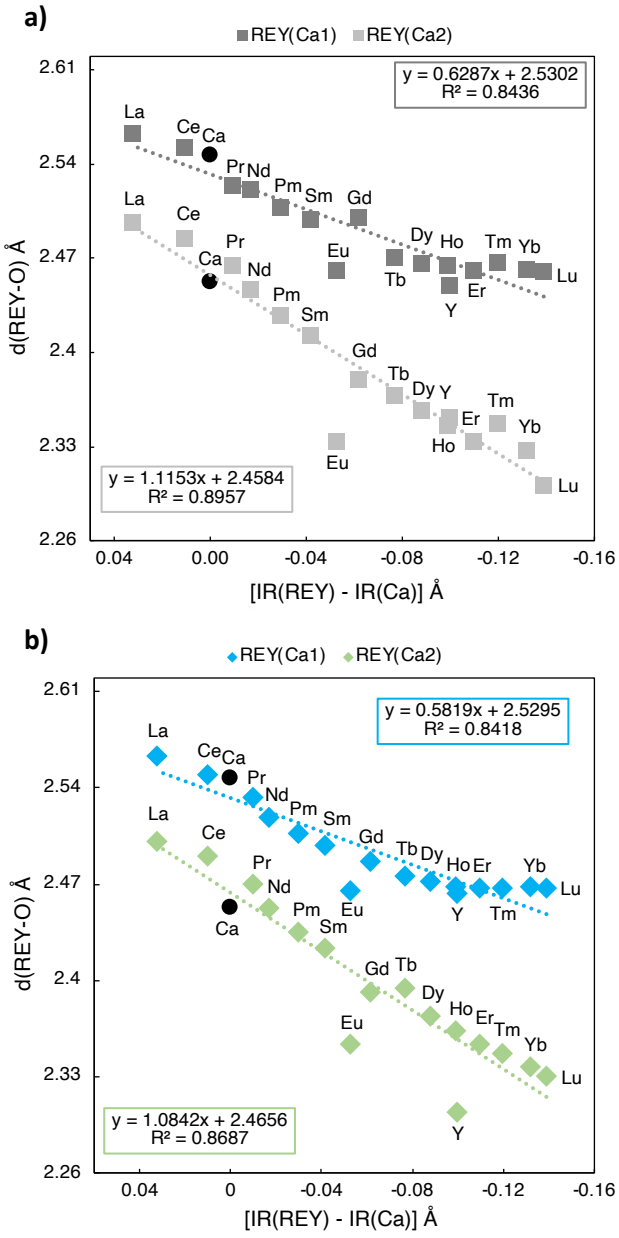

Figure 4: Variation of the average REY-O distances with the effective ionic radius in FAp for the Na (a) and Si (b) co-dopants at REY concentration of 12,500 ppm. All IR values are for the six-fold coordination. For reference purpose, the Ca-O distances are also reported on the graph, but are not included in the linear regressions.

Site Preference and effect of REY concentration. The preferred site occupancy of REY was assessed from the difference in energy between the Ca2 and Ca1 site occupancies (E(REY2) – E(REY1)). The energy difference, reported in **Figure S5** for 12,500 ppm REY**,** shows that REY are always preferably incorporated in Ca2 with Si as co-substituent. Charge compensation with Na also favors REY entering Ca2, except for Ce, Pr, Nd, Pm, Sm and Eu, which weakly prefer Ca1. To assess the influence of REY concentration on the site preference, computations were performed also at 100,000 ppm concentration (one REY atom per unit cell) and at 3,125 ppm concentration (4 x 4 x 2 supercell, **Figure 5**). As expected, a change from 12,500 ppm to 3,125 ppm marginally modifies the energetics of the site preference for all investigated compounds (<0.02 eV). REY2 is always the preferred incorporation mode regardless of the REY concentration in the case of Si charge balance. The REY2 preference is most pronounced at 100,000 ppm. In contrast to REY-Si co-doping, REY1 is preferred at 100,000 ppm for REY-Na co-doping, except for Yb and Lu for which the two sites are isoenergetic. The inversion of site preference for highly REY-Na doped FAp is due to the stabilization of the REY1 site by Na already seen at lower concentration. Results suggest that the relative site occupancies depend on the nature of the co-substituent at all concentrations, but that (locally) high REY concentrations are necessary to favor REY1 over REY2.

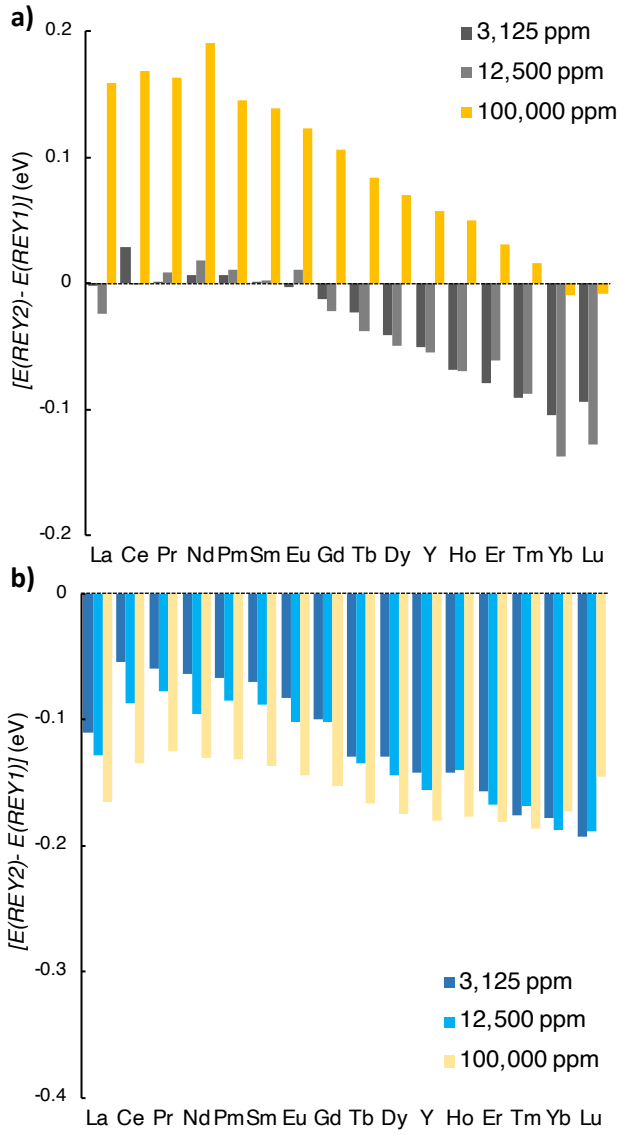

Figure 5: Effect of the concentration of REY in FAp on their site preference with Na (a) and Si (b) as co-substituent. The Ce-Na energy difference is so close to zero at 12,500 ppm, that it is not visible on the graph.

The energetics of REY clustering in FAp was estimated by calculating the reaction energy (**Δ***E*) for moving REY from a diluted to a more concentrated model. For the 12,500 ppm → 100,000 ppm reaction, the energetics is

$$\Delta E = E(\text{12,500 ppm}) + E(\text{FAp-unit-cell}) \rightarrow E(\text{100,000 ppm}) + E(\text{2x2x2-FAp}) \quad \textbf{(3)}$$

Figure 6 shows that Δ*E* is negative, which means that phase-separation is thermodynamically preferred at high REY concentration. The energy difference is about 0.05 eV for REY-Si, while it is about four times larger for REY-Na. Note that this energetic estimate does not account for configurational entropy, which would favor homogeneous, well-dispersed solid-solutions instead of phase separation. Substantial REY mobility in FAp fostered by minimization of entropic configuration requires temperatures of about 700 °C. At the temperature prevailing on the earth's surface, our computational results predict that REY tend to be clustered in FAp above ~1% concentration and at thermodynamic equilibrium.

The energetics for other reactions give a somewhat more nuanced picture. The energy difference between the 3,125 and 12,500 ppm models is now positive and does not significantly depend on whether the charge is compensated by Si or Na (**Figure S6**). This indicates minimal REY-REY interactions, as expected at relatively low concentrations. Light, and thus large in size, REY have

negligible energy difference, whereas a positive difference close to 0.1 eV is observed for heavy REY. Two effects are in competition: (i) the "size" effect, visible at 3,125 ppm, which favors dilution to accommodate the size-mismatch of the REY in the substituted site, and (ii) dopant clustering, visible at 100,000 ppm, which provides a better screening of charge-defects. The second effect is stronger for large, Na-compensated REYs (**Figure 6**). Finally, the enrichment from 3,125 ppm to 100,000 ppm reflects the competition between the two effects, as the reaction is essentially isoenergetic for small REY (typically Yb) (**Figure S7**). In contrast, phase separation into high concentration domains is preferred for the larger REY such as La and Ce.

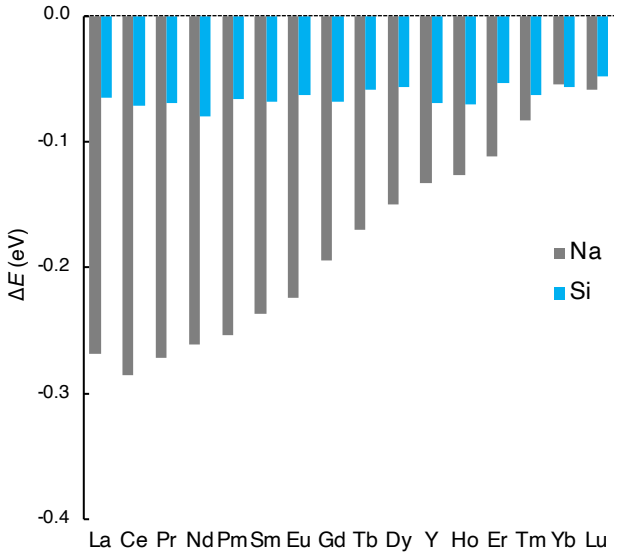

Figure 6: Reaction energy (**Δ***E)* for moving REY from the 12,500 ppm to the 100,000 ppm models.

Site Occupancy Ratios. The REY site occupancy ratios at equilibrium were calculated from the Boltzmann distribution function at 700 °C and compared to the experimental values obtained on REY-rich FAp ([REY] = 79,000 - 110,000 ppm) synthesized hydrothermally at 685-700 °C by Fleet and Pan (1995).[37] Calculations were performed at 12,500 ppm and 100,000 ppm for direct comparison with experimental values and to evaluate the dependence of the REY2/REY1 ratio on the REY concentration.

The analysis presented in **Table S3 and S4** highlights how our theoretical models compare with experimental results obtained for the four measured REY (La, Nd, Gd and Dy).[37] First of all, the site occupancy ratios for the Na and Si models at 100,000 ppm are in poor agreement with experiment: The predicted values for the Na models are below one (except for Yb and Lu), suggesting that Ca1 sites should be preferentially occupied. In contrast, the four measured REY preferred the Ca2 site. The reverse affinity is observed for the Si models. They predict Ca2/Ca1 site occupancy ratios of about eight, compared to ratios between 1-4 observed experimentally. In addition, discrepancy between observation and prediction is compounded by significant concentration effects, particularly for the Na models (**Figure 5**). This disagreement is, however, not entirely surprising given that elemental analysis of the four measured REY suggests about 40% Si and 60% Na charge compensation and that the concentration of REY varied between 0.5 (Dy) and 0.8 (Nd) for 9 Ca in the unit cell (our 100,000 ppm models correspond to 1 REY and 9 Ca). The results for the 12,500 ppm models are in better agreement with experiment. For La and Nd, the Si models fairly match experimental values. For Gd, a mixed (Na+Si) model would bring theory and experiment into agreement. Finally, for Dy, the Na models well match experimental values. This comparison illustrates the challenges: Intermediate concentrations and mixed Si/Na co-doped models could be necessary to yield good agreement between theory and experiment. Overall, concentration effects are found to be important, cautioning the use of concentrated synthetic samples to understand dilute natural samples. This becomes more important in view of the trends for Na and Si models that diverge at high REY concentration, as discussed previously.

Controls on REY Site Occupancy. The major controls on REY site occupancy have generally been interpreted in terms of the respective size of the Ca1 and Ca2 sites, although a thorough understanding is still lacking. **Figure 7** shows that the site preference, expressed as the E(REY2)-E(REY1) energy difference, varies quadratically with IR. The second-degree polynomial coefficient of determination is >0.9 for both Na and Si. Interestingly, the shape of this curve is reminiscent of the Onuma diagrams,[38–41] which are used in geochemistry to describe empirically the controlling influence of ionic radii and valence-state of substitutional doping atoms on partitioning coefficients during crystallization of a mineral from a melt or fluid. In Onuma diagrams, the parabolic shape indicates that the energetic cost for doping increases in both directions, i.e., larger and smaller atoms or ions are disfavored compared to atoms that minimize the size mismatch. Our representation is quite different from the usual Onuma diagrams, however, because we are not computing partitioning coefficients with respect to the melt, but *relative site preferences* for the same material and same dopant in an isovalent series. It is noteworthy that the maximum of the parabola in **Figure 7** is roughly located near to zero on the x-axis, where the REY and Ca have similar size. Despite a certain degree of uncertainty, a shift of about 0.02 Å towards smaller REY radii is observed. This suggests that the "nominal" size difference between the Ca1 (larger) and Ca2 (smaller) sites does not lead to a marked site preference for REY: both larger and smaller REY have a preference for the Ca2 site. Still, the small shift of the maximum to smaller REY radii is in line with the Ca2 site being smaller.

The physical parameters underlying explanations for Onuma diagrams are considered to be the excess of elastic strain energy and the dielectric polarization energy. The latter depends only weakly on the size of the substituent. Hence, it is mostly the elastic strain energy that is responsible for the Ca2 site preference as a function of IR. As described previously, the O-coordination environment of the Ca2 site is about twice as flexible as that of the Ca1 site. Hence, together with the flexible F^- coordination, as attested by the existing solid-solutions and exchanges between fluor- (F), hydroxy- (OH), and chlor- (Cl) ligands in apatite, the effective (local) elastic constant of the Ca2 site is likely lower than that of the Ca1 site. The lower stiffness of the Ca2 site derived from DFT calculation is explained structurally by the high flexibility of the corner-sharing Ca2-Ca2-Ca2 polyhedral chains (**Figure 1**). This finding could well explain the preferred incorporation of REY in the Ca2 site.

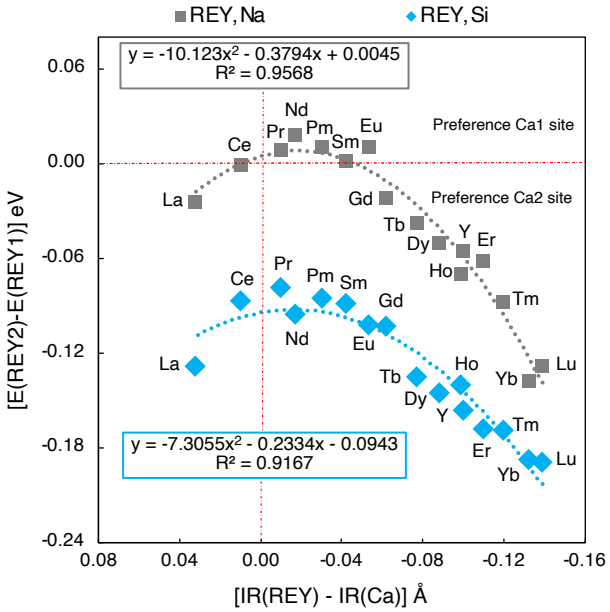

Figure 7: Variation of the site preference of REY in FAp with their effective ionic radius (IR) at REY concentration of 12,500 ppm. All IR values are for the six-fold coordination.[20,21]

The observation that the Ca2 site is (intrinsically) preferred even for cations with nearly the same size as Ca (which by definition is present in the Ca1 and the Ca2 site), such as Ce and Pr, urges for an

explanation. The Ca1 and Ca2 sites differ in their degrees of ionicity (0.429 e and 0.475 e, respectively).[24] Therefore, just like for divalent ions,[24] the ionization energies of REY may also influence the site preference. **Figure 8** shows that the site preference is linearly correlated with the sum of the first and second ionization energies with coefficients of determinations of $R^2 = 0.77$ for the Na models and $R^2 = 0.73$ for the Si models. The correlation is lower with the second ionization energy alone ($R^2 = 0.72$ for Na and $R^2 = 0.66$ for Si, **Figure S8**) and weak with the sum of the first, second, and third ionization energies ($R^2 = 0.31$-0.37, **Figure S8**). The regression slope is negative, which indicates that REY which are more difficult to ionize than Ca prefer the more ionic Ca2 site in FAp. In our previous study,[24] we found the reverse relationship for divalent cations: those which are more difficult to ionize than Ca (e.g., Mg and Cd) prefer the Ca1 site, whereas those which are more easily ionized prefer the Ca2 site (e.g., Ba and Sr). The opposite trend can be rationalized by recalling that trivalent ions are naturally more ionic than divalent ions. Therefore, they are generally better stabilized in the most ionic site (Ca2). On the other hand, divalent ions, which are less prone to lose their electrons, favor the less ionic Ca1 site.

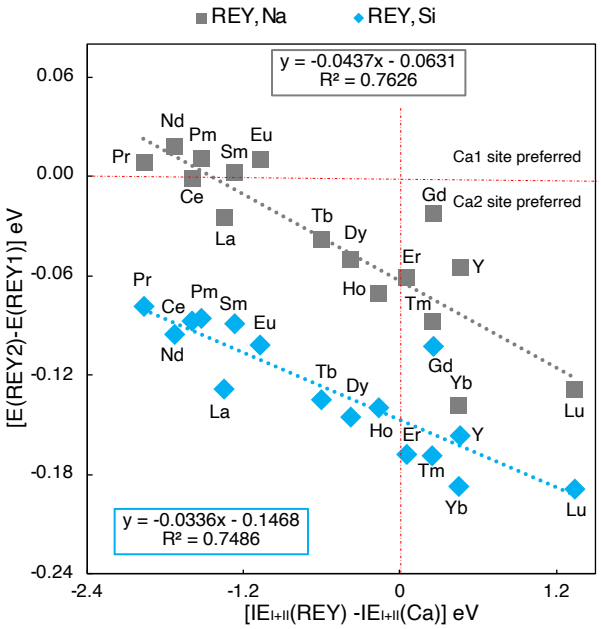

Figure 8: Relationship between the site preference of REY in FAp and the sum of their first and second ionization energies at REY concentration of 12,500 ppm.

CONCLUSIONS

This work presents a detailed theoretical study of the incorporation of REY in FAp. REY are intrinsically better stabilized in the more ionic and smaller Ca2 than in the Ca1 site with a Si co-dopant in close proximity (< 4 Å). Charge compensation with Na in a Ca1 site close to REY stabilizes the light REY in the Ca1 site at low and medium doping level (3,125-12,500 ppm) and all REY, except Yb and Lu, at high REY concentration (100,000 ppm). The enrichment reaction is exothermic from 12,500 ppm to 100,000 ppm for all REY, suggesting that there is a thermodynamic driving force for phase-separation at ambient temperature. Deviation of Yb and Lu from this trend suggests a competition between favorable interactions among REY atoms leading to clustering, on one hand, and size-mismatch effects that are easier to accommodate when REY are dispersed in the FAp structure, on the other hand.

A quadratic correlation, reminiscent of Onuma diagrams, was found between the energetics of the site preference and the ionic radius at 12,500 ppm. The top of the parabola, where stabilization in Ca2 is minimum, peaks where the REY and Ca have similar effective ionic radii. The Onuma-shape of the ionic radius dependence of the site preference suggests that the Ca2 site is more flexible (i.e., has lower effective elastic constant) than the Ca1 site, which is also supported by the slope of the REY-O coordination distance as a function of the ionic radius. Being linked through corners, the Ca2 polyhedra

are more apt to deform than the face-sharing Ca1 polyhedra. Furthermore, the Ca2 site preference was found to depend linearly on the ionization energy of REY. Noteworthily, the stabilization energy in the Ca2 site increases with the ionization energy for trivalent REY cations, whereas it decreases with the ionization energy for divalent cations.[24] In summary, ionization energies of REY, together with the lower effective elastic constant of the Ca2 site compared to the Ca1 site, i.e., Ca2 is intrinsically more apt to stabilize differently sized ions, appear to be the two main thermodynamic driving forces for their partitioning between the Ca1 and Ca2 sites.

ASSOCIATED CONTENT

Supporting Information

Experimental and DFT lattice parameters; Ca2/Ca1 occupancy ratio at 12,500 ppm and 100,000 ppm; stabilization energy of REY in the Ca2 and Ca1 sites for the “far” and “close” models; site preference of REY for Si for P and in Na for Ca coupled substitutions in the “close” model; relationship between unit-cell volume and REY IR and site preference; reaction energies between the 3,125 ppm, 12,500 ppm, and 100,000 models; variation of site preference against ionization energy; variation of the REY-O distance against IR. All computations are available under doi.org/10.17172/NOMAD/2025.04.16-1

AUTHOR INFORMATION

ACKNOWLEDGEMENTS

Financial support was provided by the European Union (ERC, Advanced Grant DEEP-SEE, 101052913). Views and opinions expressed are however those of the authors only and do not necessarily reflect those of the European Union or the European Research Council Executive Agency. Neither the European Union nor the granting authority can be held responsible for them. We acknowledge support from the CBPsmn (PSMN, Pôle Scientifique de Modélisation Numérique) of the ENS de Lyon for the computing resources.

REFERENCES

(1) Nash, W. P. Phosphate Minerals in Terrestrial Igneous and Metamorphic Rocks. In *Phosphate Minerals*; Nriagu, J. O., Moore, P. B., Eds.; Springer-Verlag, 1984; p 442.
(2) Harlov, D. E.; Rakovan, J. F. *Apatite: A Mineral for All Seasons*; Elements; 2015; Vol. 11.
(3) Liao, J.; Sun, X.; Li, D.; Sa, R.; Lu, Y.; Lin, Z.; Xu, L.; Zhan, R.; Pan, Y.; Xu, H. New Insights into Nanostructure and Geochemistry of Bioapatite in REE-Rich Deep-Sea Sediments: LA-ICP-MS, TEM, and Z-Contrast Imaging Studies. *Chem. Geol.* **2019**, *512*, 58–68.
(4) Jiang, X.; Sun, X.; Chou, Y.; Hein, J.; He, G.; Fu, Y.; Li, D.; Liao, J.; Ren, J. Geochemistry and Origins of Carbonate Fluorapatite in Seamount Fe-Mn Crusts from the Pacific Ocean. *Mar. Geol.* **2020**, *423*, n° 106135.
(5) Bi, D.; Shi, X.; Huang, M.; Yu, M.; Zhou, T.; Zhang, Y.; Zhu, A.; Shi, M.; Fang, X. Geochemical and Mineralogical Characteristics of Deep-Sea Sediments from the Western North Pacific Ocean: Constraints on the Enrichment Processes of Rare Earth Elements. *Ore Geol. Rev.* **2021**, *138*, n° 104318.
(6) Liao, J.; Chen, J.; Sun, X.; Wu, Z.; Deng, Y.; Shi, X.; Wang, Y.; Chen, Y.; Koschinsky, A. Quantifying the Controlling Mineral Phases of Rare-Earth Elements in Deep-Sea Pelagic Sediments. *Chem. Geol.* **2022**, *595*, n° 120792.
(7) Manceau, A.; Paul, S.; Simionovici, A.; Magnin, V.; Balvay, M.; Findling, N.; Rovezzi, M.; Muller, S.; Garbe-Schonberg, D.; Koschinsky, A. Fossil Bioapatites with Extremely High Concentrations of Rare Earth Elements and Yttrium from Deep-Sea Pelagic Sediments. *ACS Earth Space Chem.* **2022**, *6*, 2093–2103.
(8) Kato, Y.; Fujinaga, K.; Nakamura, K.; Takaya, Y.; Kitamura, K.; Ohta, J.; Toda, R.; Nakashima, T.; Iwamori, H. Deep-Sea Mud in the Pacific Ocean as a Potential Resource for Rare-Earth Elements. *Nature Geosci.* **2011**, *4*, 535–539.

(9) Kon, Y.; Hoshino, M.; Sanematsu, K.; Morita, S.; Tsunematsu, M.; Okamoto, N.; Yano, N.; Tanaka, M.; Takagi, T. Geochemical Characteristics of Apatite in Heavy REE-Rich Deep-Sea Mud from Minami-Torishima Area, Southeastern Japan. *Res. Geol.* **2014**, *64*, 47–57.
(10) Balaram, V. Rare Earth Elements: A Review of Applications, Occurrence, Exploration, Analysis, Recycling, and Environmental Impact. *Geosci. Front.* **2019**, *10*, 1285–1303.
(11) Hughes, J. M.; Rakovan, J. The Crystal Structure of Apatite, $Ca_5(PO_4)_3(F,OH,Cl)$. In *Phosphates: Geochemical, Geobiological, and Materials Importance*; Kohn, M. J., Rakovan, J., Hughes, J. M., Eds.; Rev. Miner. Geochem.; 2002; Vol. 48, pp 1–12.
(12) Hughes, J. M.; Cameron, M.; Crowley, K. D. Structural Variations in Natural F, OH, and Cl Apatites. *Am. Miner.* **1989**, *74*, 870–876.
(13) Mackie, P. E.; Young, R. A. Location of Nd Dopant in Fluorapatite, $Ca_5(PO_4)_3F$:Nd. *J. Appl. Cryst.* **1973**, *6*, 26–31.
(14) Fleet, M. E.; Pan, Y. Site Preference of Nd in Fluorapatite [$Ca_{10}(PO_4)_6F_2$]. *J. Sol. State Chem.* **1994**, *112*, 78–81.
(15) Bertolus, M.; Defranceschi, M. Optimizing the Formula of Rare Earth-Bearing Materials: A Computational Chemistry Investigation. *Int. J. Quantum Chem.* **2000**, *107*, 712–721.
(16) Get'man, E. I.; Loboda, S. N.; Tkachenko, T. V.; Yablochkova, N.; Chebyshev, K. Isomorphous Substitution of Samarium and Gadolinium for Calcium in Hydroxyapatite Structure. *Russ. J. Inorg. Chem.* **2010**, *55* (3), 333–338.
(17) Alshemary, A. Z.; Akram, M.; Goh, Y. F.; Kadir, M. R. A.; Abdolahi, A.; Hussain, R. Structural Characterization, Optical Properties and in Vitro Bioactivity of Mesoporous Erbium-Doped Hydroxyapatite. *J. Alloys. Compd.* **2015**, *645*, 478–486.
(18) Hughes, J. M.; Cameron, M.; Mariano, A. N. Rare-Earth-Element Ordering and Structural Variations in Natural Rare-Earth-Bearing Apatites. *Am. Miner.* **1991**, *76*, 1165–1173.
(19) Fleet, M. E.; Pan, Y. M. Crystal-Chemistry of Rare-Earth Elements in Fluorapatite and Some Calc-Silicates. *Eur. J. Miner.* **1995**, *7*, 591–605.
(20) Shannon, R. D.; Prewitt, C. T. Effective Ionic Radii in Oxides and Fluorides. *Acta Cryst.* **1969**, *B25*, 925–945.
(21) Shannon, R. D. Revised Effective Ionic Radius and Systematic Studies of Interatomic Distances in Halides and Chalcogenides. *Acta Crystallogr.* **1976**, *B25*, 925–946.
(22) Pan, Y.; Fleet, M. Compositions of the Apatite-Group Minerals: Substitution Mechanisms and Controlling Factors. In *Phosphates: Geochemical, Geobiological, and Materials Importance*; Kohn, M., Rakovan, J., Hughes, J., Eds.; 2002; Vol. 48, pp 13–49.
(23) Rønsbo, J. G. Coupled Substitutions Involving REEs and Na and Si in Apatites in Alkaline Rocks from the Ilimaussaq Intrusion, South Greenland, and the Petrological Implications. *Am. Miner.* **1989**, *74*, 896–901.
(24) Manceau, A.; Mathon, O.; Lomachenko, K. A.; Rovezzi, M.; Kvashnina, K. O.; Boiron, M. C.; Brossier, R.; Steinmann, S. N. Revealing the Incorporation of Cerium in Fluorapatite. *ACS Earth Space Chem.* **2024**, *8*, 119–128.
(25) Sham, L. J.; Schlüter, M. Density-Functional Theory of the Energy Gap. *Phys. Rev. Lett.* **1983**, *51*, 1888–1891.
(26) Blochl, P. E. Projector Augmented-Waves Method. *Phys. rev. B.* **1994**, *50*, 17953–17979.
(27) Kresse, G.; Joubert, D. From Ultrasoft Pseudopotentials to the Projector Augmented-Wave Method. *Phys. Rev. B.* **1999**, *59*, 1758–1775.
(28) Kresse, G. Ab-Initio Molecular-Dynamics for Liquid Crystals. *J. Non-Cryst. Solids* **1995**, *193*, 222–229.
(29) Kresse, G.; Furthmuller, J. Efficiency of Ab-Initio Total Energy Calculations for Metals and Semiconductors Using a Plane-Wave Basis Set. *Comput. Mater. Sci.* **1996**, *6*, 15–50.
(30) Quemener, E.; Corvellec, M. SIDUS—the Solution for Extreme Deduplication of an Operating System. *Linux J.* **2013**, *2013* (235), 3:3.
(31) Perdew, J. P.; Ernzerhof, M. Rationale for Mixing Exact Exchange with Density Functional Approximations. *J. Chem. Phys.* **1996**, *105*, 9982–9985.
(32) Steinmann, S. N.; Corminboeuf, C. Comprehensive Benchmarking of a Density-Dependent Dispersion Correction. *J. Chem. Theory Comput.* **2011**, *7*, 3567–3577.
(33) Gautier, S.; Steinmann, S. N.; Michel, C.; Fleurat-Lessard, P.; Sautet, P. Molecular Adsorption at Pt(111). How Accurate Are DFT Functionals? *Phys. Chem. Chem. Phys.* **2015**, *17*, 28921–28930.
(34) Perdew, J. P.; Wang, Y. Accurate and Simple Analytic Representation of the Electron-Gas Correlation Energy. *Phys. Rev. B* **1992**, *45* (23), 13244–13249.

(35) Roy, A.; Kanungo, B.; Patra, P. K.; Bhattacharya, B. Benchmarking DFT Approximations for Studying Apatites. *Phys. Chem. Chem. Phys.* **2024**, *26* (47), 29617–29627. https://doi.org/10.1039/D4CP03169E.
(36) Chiatti, F.; Delle Piane, M.; Ugliengo, P.; Corno, M. Water at Hydroxyapatite Surfaces: The Effect of Coverage and Surface Termination as Investigated by All-Electron B3LYP-D* Simulations. *Theor Chem Acc* **2016**, *135* (3), 1–15. https://doi.org/10.1007/s00214-016-1818-8.
(37) Fleet, M. E.; Pan, Y. M. Site Preference of Rare-Earth Elements in Fluorapatites. *Am. Miner.* **1995**, *80*, 329–335.
(38) Onuma, N.; Higuchi, H.; Wakita, H.; Nagasawa, H. Trace Element Partition between Two Pyroxenes and the Host Lava. *Earth Planet. Sci. Lett.* **1968**, *5*, 47–51.
(39) Blundy, J.; Wood, B. Prediction of Crystal-Melt Partitioning Coefficients from Elastic Moduli. *Nature* **1994**, *372* (6505), 452–454.
(40) Blundy, J.; Wood, B. Partitioning of Trace Elements between Crystals and Melts. *Earth Planet. Sci. Lett.* **2003**, *210*, 383–397.
(41) Karato, S. Physical Basis of Trace Element Partitioning: A Review. *Am. Miner.* **2016**, *101*, 2577–2593.

TABLE OF CONTENT GRAPHIC